Chemistry & Biology, Vol. 11, 1119–1126, August, 2004, ©2004 Elsevier Ltd. All rights reserved. DOI 10.1016/j.chembiol.2004.05.021

Crystal Structure of a Continuous Three-Dimensional DNA Lattice

Paul J. Paukstelis,[1,*] Jacek Nowakowski,[1] Jens J. Birktoft,[2] and Nadrian C. Seeman[2]
[1]Institute for Cellular and Molecular Biology
University of Texas at Austin
1 University Station A4800
Austin, Texas 78712
[2]Department of Chemistry
New York University
100 Washington Square East
New York, New York 10003

Summary

DNA has proved to be a versatile material for the rational design and assembly of nanometer scale objects. Here we report the crystal structure of a continuous three-dimensional DNA lattice formed by the self-assembly of a DNA 13-mer. The structure consists of stacked layers of parallel helices with adjacent layers linked through parallel-stranded base pairing. The hexagonal lattice geometry contains solvent channels that appear large enough to allow 3′-linked guest molecules into the crystal. We have successfully used these parallel base pairs to design and produce crystals with greatly enlarged solvent channels. This lattice may have applications as a molecular scaffold for structure determination of guest molecules, as a molecular sieve, or in the assembly of molecular electronics. Predictable non-Watson-Crick base pairs, like those described here, may present a new tool in structural DNA nanotechnology.

Introduction

Rational design and assembly of nanometer-size molecular objects has been a major goal of supramolecular chemistry and nanotechnology. A variety of molecular building blocks have been successfully used in the programmed assembly of nanoscale structures (e.g., [1–3]). One of the most successful of these has been DNA. Constructions of complex topology, including a cube, Borromean rings, and two-dimensional tiled sheets have been created with DNA [4]. Several examples of nanomechanical devices constructed from DNA have also been reported [5–7]. One important goal of structural DNA nanotechnology has been the engineering of a three-dimensional DNA lattice [8].

DNA has several features that make it an excellent building block for the construction of nanometer-scale structures. First, interstrand cohesion mediated by Watson-Crick base pairing provides predictability to duplex DNA interactions and to helix geometry [9]. Base pairing provides rational programmability for DNA duplex formation in a complex structure. The DNA double helix is stiff over short distances [10], allowing for predictable lengths and orientations during assembly. DNA of designed sequence is easily synthesized through phosphoramidite chemistry [11], both as the conventional structure and as modified derivatives.

The Watson-Crick DNA double helix axis is topologically linear; the ability to form complex structures from DNA requires branching from these lines [4]. Branched DNA occurs naturally during recombination in the form of Holliday junctions, and several designs have used asymmetric sequences, programmed by Watson-Crick base pairs, to create nonmigratory branched junctions. Multiple-crossover motifs have been designed to self-assemble in a variety of two-dimensional arrays based on the Watson-Crick pairing of sticky ends [12]. Biological examples of structurally complex nucleic acids are not limited to Watson-Crick interactions. Nonstandard base pairs play a crucial role in the formation of the functional tertiary structures for a variety of RNA molecules [13, 14] including tRNA molecules, rRNA molecules, and RNA introns. For DNA, sequences within telomeric repeats of chromosomal DNA are known to produce nonstandard base pairs, such as G-tetraplex structures [15]. DNA triplet repeat expansions, implicated in a number of human diseases, have also been postulated to form nonstandard pairs [16]. Non-Watson-Crick base pairs are thermodynamically less favorable than canonical pairings [17], but they appear readily in the absence of opportunities for Watson-Crick pairing or in favorable environments. Their formation, while not always predictable, provides structural diversity that in some cases is required for biological function. In the case of RNA molecules, the formation of non-Watson-Crick base pairs is key to proper folding [14] and to RNA recognition by proteins and other ligands [18]. Predictable non-Watson-Crick base pairs may provide a similar structural diversity for the creation of DNA nanoscale motifs.

Here we present the 2.1 Å crystal structure of a 13-nucleotide DNA molecule, d(GGACAGATGGGAG), that self-assembles into a three-dimensional lattice through base pairing and base stacking interactions. This DNA sequence was designed to form a duplex with a biotinylated complementary DNA strand tethered to streptavidin, as part of a tripartite complex. During crystallization trials, the oligonucleotide crystallized by itself, excluding the complementary DNA-streptavidin complex. Although this DNA crystal has not been designed rationally, it provides a unique look at alternatives to Watson-Crick base pairing in DNA self-assembly and fortuitously solves the problem of creating a porous three-dimensional DNA lattice for potential nanotechnological applications. Using this structure as a framework, we have successfully engineered three-dimensional crystals with altered lattice dimensions.

Results and Discussion

Overview of the DNA Lattice Structure

The overall geometry of the DNA lattice can be visualized as three repeating layers of parallel helices, with each

*Correspondence: paul@intron.icmb.utexas.edu

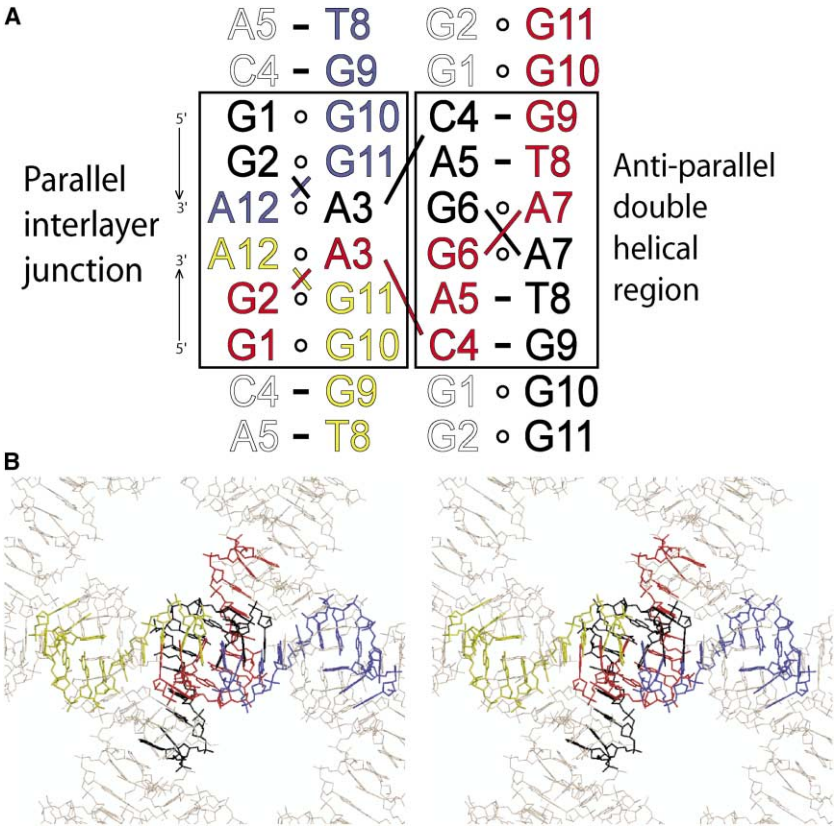

Figure 1. Two- and Three-Dimensional Representations of a Continuous DNA Lattice

(A) The secondary structure of the 3D DNA array highlighting the two regions of base pairing and the stacking interactions that make up the lattice. Four strands, all of which are related by crystallographic symmetry, are colored differently to highlight the base pairing relationship between them. The double helical region forms via antiparallel base pairing and contains a dyad axis between the central G-A mismatch base pairs. The interlayer junction forms three parallel-stranded homopurine base pairs, with two sets of these interactions stacked upon a 2-fold axis. Only the phosphate of G13 was present in electron density, and it has been omitted for clarity. Open circles between base pairs represent noncanonical pairings. Dashes indicate Watson-Crick base pairs.

(B) A stereo image showing the three-dimensional relationship of the same four strands shown in (A) viewed down the dyad axis.

layer rotated 60° relative to the flanking layers (Figure 1). Each layer is composed of coaxially stacked pseudo-infinite helices separated by 20 Å of solvent space. These stacked helices interact with adjacent layers through parallel-stranded base pairing at the regions of coaxial stacking. Each DNA monomer forms base pairs with three identical strands related by crystallographic symmetry, yielding six unique base pairs within two regions of pairing (Figure 1A). The helical region forms an antiparallel double helix of B-form geometry through the base pairing of C4-G9 from two monomers. The phosphodiester backbone turns sharply between residues C4 and A3, moving G1-G2-A3 out of the axis of the helical region; this feature allows G1-G2-G3 to pair with G10-G11-A12, respectively, of a monomer in an adjacent layer. These parallel-stranded homopurine base pairs form an interlayer junction that connects each two-dimensional layer into a continuous three-dimensional array. The 20 Å spacing between the parallel helices within each layer creates an internal network of solvent channels (Figure 2). These channels run parallel with and perpendicular to the 6_4 symmetry axis through the length of the crystal. The channels parallel to the 6-fold axis have a circular area of ~300 Å^2 in projection and a volume of ~17,500 Å^3 per unit cell. Each of the channels running perpendicular to the 6-fold axis has an area of ~360 Å^2 and a volume of ~14,600 Å^3 per unit cell. These perpendicular channels intersect the parallel channel, and they share ~5500 Å^3 per unit cell. The base and ribose of the 3′-terminal residue, G13, appear to be oriented into the channel intersection and could not be seen in the electron density maps.

Antiparallel Double Helical Region

The double helical region contains three unique base pairs formed by the antiparallel base pairing of C4-G9 of two monomers (Figure 3). This region consists of two repeated sets of these pairings about a dyad axis between the central G6-A7 mispairs. The two outermost pairs are formed by C4-G9 and A5-T8 and are the only two Watson-Crick pairs in this structure. The Watson-Crick pairs flank two sheared G6-A7 pairs. The crystal structure of the oligonucleotide d(CCAAGATTGG) contains two similar Watson-Crick-flanked sheared G-A pairs, and comparison of the four central bases from the X-ray structure of this molecule [19] with the helical region reveals similar local and helical parameters. The structures conform well to canonical B-form DNA pa-

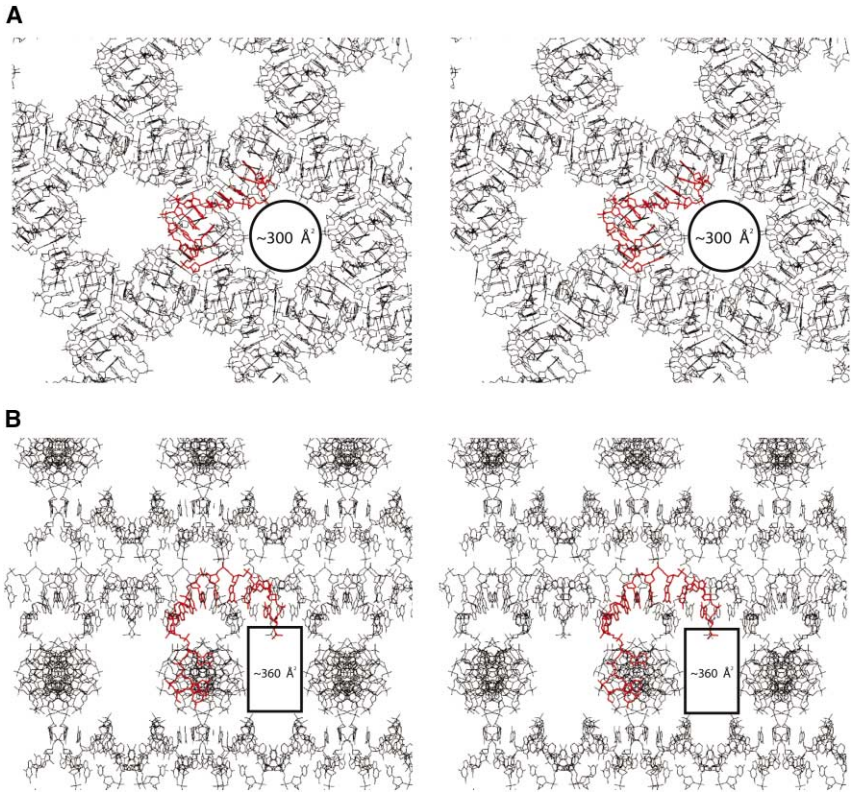

Figure 2. Crystal Packing of d(GGACAGTGGGAG) Forms Solvent Channels that Run through the Length of the Crystal in Four Directions

(A) A stereoview down the 6-fold axis showing the hexagonal channels running the length of the crystal. For reference, a monomer is colored in red. These channels have a cross-sectional area of ~300 Å^2 using the G9 phosphate-G9 phosphate distance across the channels as the diameter.

(B) A stereoview orthogonal to the 6-fold symmetry axis looking down one layer of coaxially stacked helices. One set of solvent channels runs parallel to each helical layer, resulting in three sets of solvent channels at 60° to each other. These channels have a cross-sectional area of ~360 Å^2. The channels in (A) and (B) intersect and share a volume of ~5800 Å^3. All measurements are based on atom-atom distances.

rameters and compensate for the non-Watson-Crick pair by x-displacement as determined using 3DNA software [20]. Large propeller values for the G-A pairs and the flanking A-T pairs (−25.5° and −24.0°, respectively) are stabilized by a hydrogen bond between N2 of G6 and the O2 of the flanking T8. This same interstrand hydrogen bond is observed in the d(CCAAGATTGG) structure. Base stacking in the helical region is uninter-

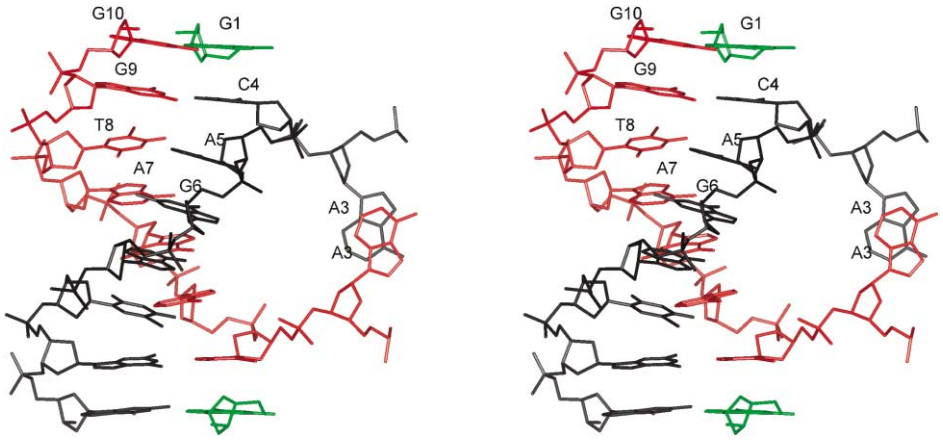

Figure 3. A Stereo Figure of the Double Helical Region

The helical region contains two sets of three unique base pairs. C4 does not stack continuously with the helical region, but does stack with G1 from another monomer, shown in green. The minor groove is on the left, the major groove on the right. The major groove is partially obstructed by the sharp bend between A3 and C4.

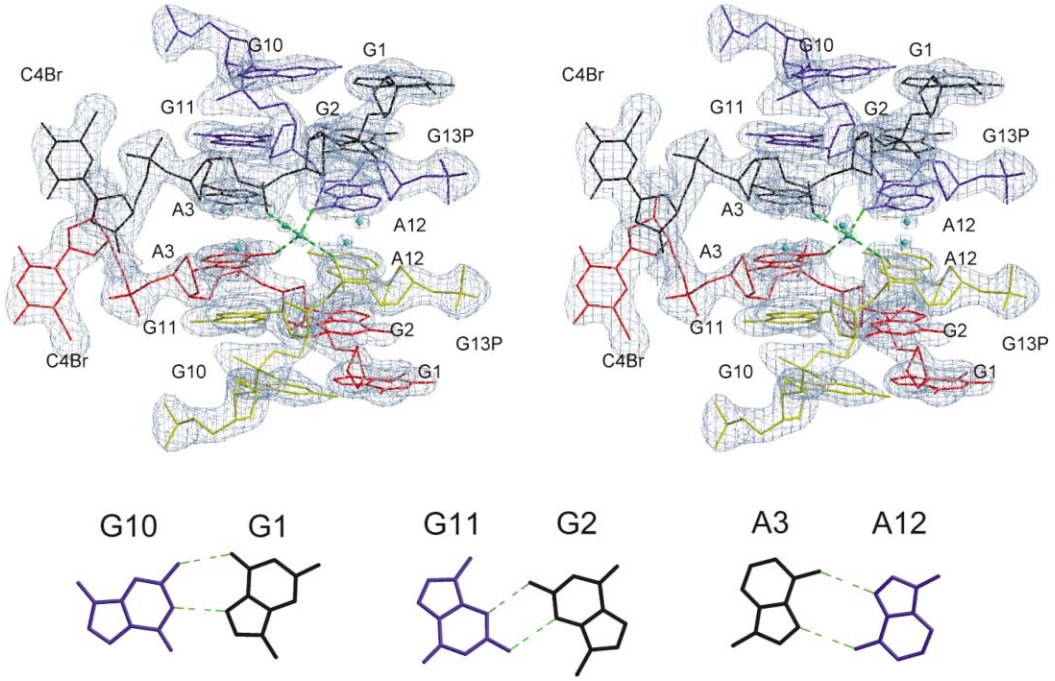

Figure 4. Stereo Figure of the Interlayer Junction

Solvent-flattened experimental electron density contoured at 1.5 σ. Each of the four strands making up the junction is colored differently, as in Figure 1. Blue spheres indicate solvent molecules hydrating the junction. Dashed green lines represent the solvent-mediated hydrogen bonding between phosphate oxygen atoms with A3 and A12 bases across the 2-fold symmetry axis. The lower panel images show a top-down view of the hydrogen bonding between the parallel base pairs. Figures were generated with Xfit [33], Raster3D [35], and InsightII (Accelyrs).

rupted from A5 to G9, but a backbone distortion resulting in a large y-displacement between A3 and C4 moves the C4 base out of this helical axis, preventing intrastrand stacking with A5. This sharp bend is accompanied by a slight inclination of the C4-G9 pair, resulting in a partial closure of the major groove. While C4 does not stack with any bases from the helical region, it does stack with G1 from a molecule in an adjacent layer (Figure 3).

Interlayer Region Composed of Non-Watson-Crick Base Pairs

The interlayer region is composed of two symmetry-related sets of three homopurine base pairs that stack about a 2-fold axis and act as connections between helical layers to generate the three-dimensional lattice (Figure 4). The outermost mismatch from this symmetry axis, G1-G10, is stabilized by two hydrogen bonds between the major groove edge of G1 and the Watson-Crick edge of G10. The intermediate pairing is formed by G2-G11 via symmetrical N2-N3 hydrogen bonding of the minor groove edges. The innermost pair, A3-A12, is also symmetrical, through N6-N7 hydrogen bonding. Two A3-A12 pairs stack about a 2-fold axis perpendicular to the parallel-stranded helix axis formed by the ends of the four strands. This provides the end-to-end stacking responsible for generating the pseudoinfinite nature of each helical layer. Intrastrand base stacking is continuous from A5 of the double helical region through G10 of the interlayer junction, but is interrupted by the staggering of the G2-G11 pair. This base pair displays cross-strand stacking; G11 stacks with A3 from its partner strand, and G2 stacks with the A12 of its partner strand. This feature is represented schematically in Figure 1A. Along with base stacking, solvent-mediated base-backbone hydrogen bonding provides additional stability across the 2-fold axis. N6 amino groups from nonpartner A3 and A12 bases form a shared hydrogen bond with a well-ordered solvent molecule. This solvent molecule serves to bridge phosphate oxygens from hydrogen bonded A3 and A12 partners. This molecule belongs to a group of well-ordered solvent molecules that hydrate the 2-fold junction (Figure 4).

Comparison of the temperature factors between the interlayer junction and helical region suggests that the non-canonical parallel region is better ordered than the near-B-form double helical region. The average B factor for the six residues in the interlayer junction is 35 Å^2, while the average for the six residues of the double helical region is 48 Å^2. This ordering likely reflects the strong stacking interactions between bases in this region.

Comparisons to Other Parallel DNA Structures

Creation of nanoscale objects from DNA requires the predictability of hydrogen bonding interactions between strands and the formation of a coherent local product structure from these interactions. Comparing the structure described here with parallel-stranded DNA structures containing 5′-GGA or 5′-CGA parallel regions indi-

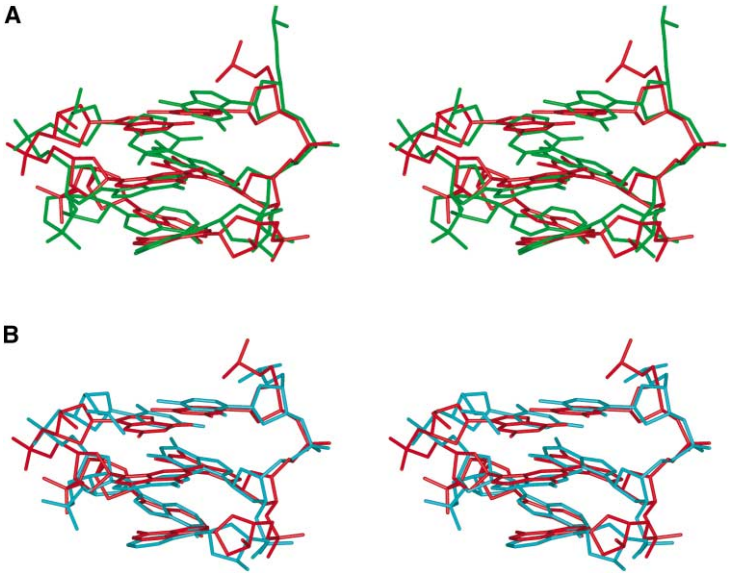

Figure 5. Structural Comparision of Homo Parallel Base Pairs

(A) The interlayer junction is structurally similar to the V-shaped arrowhead motif. The unique pairs of the interlayer junction are in red, and a representative model of the arrowhead motif (PDB: 1B3P) is shown in green.

(B) Homo parallel regions with the sequence 5′-GGA and 5′-CGA are structurally congruent. The three unique pairs of the interlayer junction are shown in red, and the first three parallel bases in the crystal structure of d(GCGAAAGCT) (PDB: 1IXJ) are shown in cyan.

cates the homonucleotide base pairs found here can satisfy these requirements.

The three base pairs of the interlayer junction are virtually identical to the parallel-stranded homopurine pairs seen in the NMR structure of d(GGAGGAT) in which two symmetrical strands make up a V-shaped "arrowhead" motif [21] (Figure 5A). Both molecules use identical hydrogen bond donor and acceptor pairs. The largest differences between the base pair parameters of the two structures are in the propeller and the inclination of the outermost G1-G10 pair and likely are due to stacking forces imposed by crystal formation. The 5′-terminal guanine is in the *syn* orientation allowing for Hoogsteen pairing in both structures and appears to play an important role in stabilizing the continuous array. The pyrimidine ring of G1 stacks with C4 from the helical region of an adjacent monomer and provides stacking between the parallel and antiparallel regions of base pairing (Figures 1 and 3).

Several structural studies of molecules containing the DNA sequence 5′-CGA have observed similar parallel base pairing. In the case of these molecules, the C-C base pair requires that one cytosine residue be hemiprotonated to form symmetrical hydrogen bonds. NMR studies have confirmed pH-dependent transitions for the molecules d(CGATCG), d(TCGATCGA), and d(CGATCGATCG) [22]. The crystal structure of d(GCGAAAGCT) displays both parallel homo base pairs and antiparallel Watson-Crick pairs between symmetry related molecules, similar to the structure described here [23]. This structure forms a parallel region by the self-pairing of the second, third, and fourth nucleotides and an additional pair from the fifth nucleotide, forming a symmetrical A-A pair via two N1-N6 hydrogen bonds. Superposition of the interlayer junction and 5′-CGA parallel region from d(GCGAAAGCT) shows that these three base pairs are structurally equivalent, with minor differences noted in the 5′ pair (Figure 5B). The C(+)-C hydrogen bond interface is coincident with the parallel helix axis (in this case also a crystal axis), while the Hoogsteen base pairs in 5′-GGA parallel regions result in larger y-displacement values for the terminal G-G pairing. Importantly, all of these structures display interstrand stacking between the second and third base pairs, and in all cases these nucleotides are G and A, respectively. This strong interstrand stacking is thought to provide much of the stabilization for the parallel stranded helix [22].

One common sequence characteristic of the arrowhead motif and the interlayer junction is the presence of a 5′-terminal GGA. Our attempts to crystallize oligonucleotides with an additional 5′ nucleotide were not successful. Structural studies of another DNA oligonucleotide containing internal GGA repeats, d(GTGGAATGG AAC), find an antiparallel duplex with two unpaired guanines flanked by sheared G-A mismatch pairs [24]. The two bases 5′ to the first GGA form antiparallel Watson-Crick pairs with the last two bases. Stacking and antiparallel base pairing of these first two bases may limit the ability to adopt the parallel base pairs seen in the interlayer junction and arrowhead motifs. In the case of d(GCGAAAGCT), the 5′-CGA parallel region contains one nucleotide 5′ of the CGA. The 5′-CGA structures are likely able to accommodate this extra nucleotide due to the differences in crystal packing and the additional symmetry allowed by the 5′-terminal hemiprotonated C-C pair compared with the asymmetric G-G Hoogsteen pair.

Crystal Design Using Parallel Base Pairs

To test the use of parallel homopurine base pairs in rational DNA engineering, we designed, modeled, and crystallized a two-strand DNA lattice using the interactions observed in the structure described here. This lattice contains a variable-length insertion between the helical region and interlayer junction that is paired with a second strand to generate one full turn of antiparallel Watson-Crick helix (Figure 6A). This structure was modeled as a four-stranded dimer in $P3_1$ to avoid the difficulty of maintaining base pairing between symmetry-related molecules. Building of the symmetry-related molecules

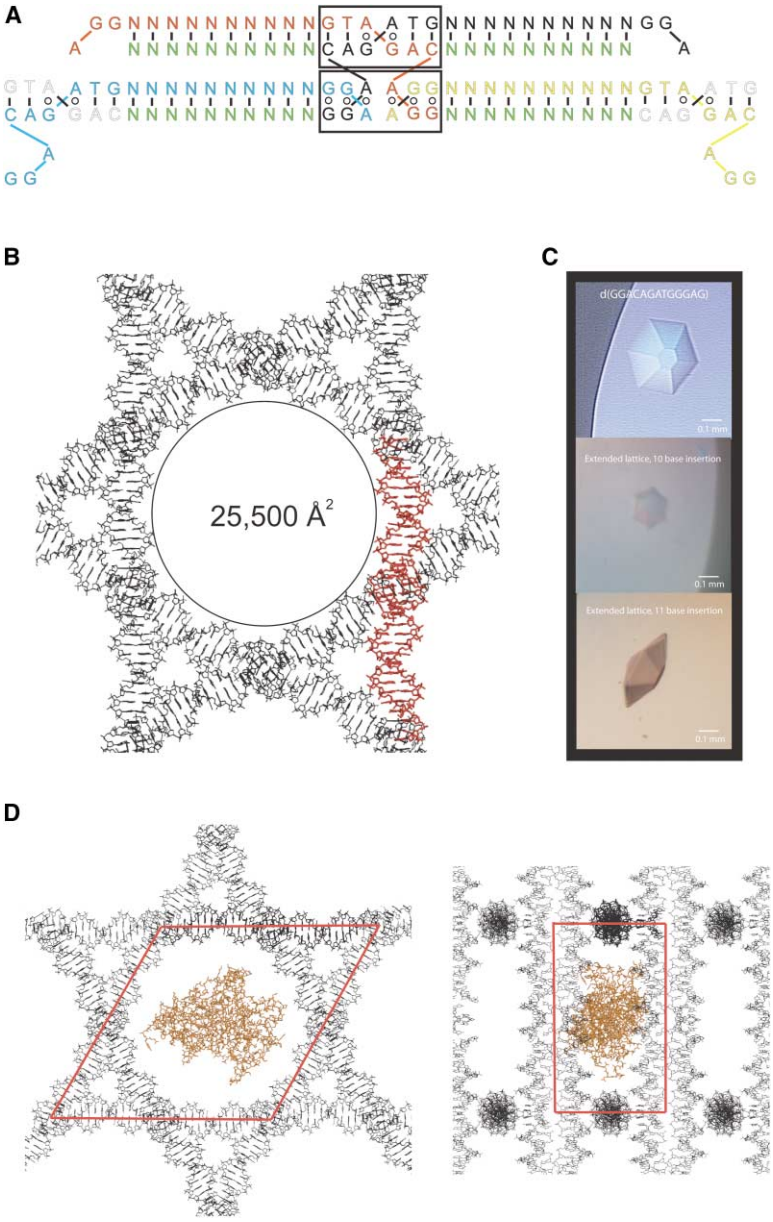

Figure 6. Design and Crystallization of an Expanded Three-Dimensional DNA Lattice

(A) The extended DNA lattice was designed by placing a 10–11 base insertion between the helical region and the interlayer junction and using a second complementary strand (green) to extend one full helical turn. The secondary structure shows the same interactions of the helical region and interlayer junction.

(B) Modeling of the extended lattice shows a large expansion of the solvent channels as seen down the 6-fold axis. This is a nearly 100-fold expansion to 25,500 Å^2. For reference, a dimer (two extended molecules and two second strands) is shown in red.

(C) Comparison of crystals produced from the 13-mer lattice and the lattice designed in (A). Both crystals show hexagonal morphology, and X-ray diffraction analysis confirmed the primitive hexagonal lattice and showed the experimental unit cell dimensions were within 3 Å of the predicted unit cell as modeled in (B).

(D) The large expansion of the solvent channels in the extend lattice could allow for it to be used as a macromolecular scaffold for whole proteins. Two orthogonal views show a 45 kDa fungal mitochondrial tyrosyl-tRNA synthetase fitting within a single unit cell outlined by the red boxes.

with a predicted unit cell that maintained all the interactions of the 13-mer structure showed a large expansion of the solvent channels running parallel to the 6-fold axis (Figure 6B). The circular area expands nearly 100-fold when viewed down the 6-fold axis (300 Å^2 to 25,500 Å^2). This results in 1.4 $\times$ 10^6 Å^3 of solvent space per unit cell in the channels running parallel to the 6-fold axis.

Crystallization trials of oligonucleotides with insertion and second strand lengths of 10 and 11 nucleotides yielded hexagonal crystals within 2 days using the same conditions as for the single-stranded lattice (Figure 6C). These crystals grew to a maximum size of 0.4 mm, with the 11 base insertion crystals being consistently larger. Denaturing polyacrylamide gel electrophoresis of washed and dissolved crystals confirmed that both strands were present in the crystals (data not shown). These crystals diffracted to 5 Å resolution at room temperature (or 100 K) and exhibited high mosaicity. However, several crystals were readily indexed, confirming the primitive hexagonal lattice; similarly, they showed an experimental unit cell within 3 Å of the predicted unit cell from modeling in all dimensions. This provides excellent evidence that the model closely resembles the actual structure. We are currently attempting to improve the diffraction of these crystals.

Potential Applications

Continuous three-dimensional DNA crystals have been recognized as one path toward a variety of nanotechnological applications. These include uses as a scaffold for structure determination of guest molecules [8], as a molecular sieve [25], and in the assembly of molecular electronic components [26]. The solvent channels run-

Table 1. Data Collection and Model Refinement Statistics

Data Set	Bromo
X-ray source	NSLS X8-C
Wavelength (Å)	0.92002
Max. resolution (Å)	2.1
Completeness (%)[a]	99.2 (99.4)
I/σ (I)	20.7 (10.7)
Multiplicity	7.0
Reflections	5516
R_{merge} (%)	7.0 (10.2)
Number of sites	2
Model Refinement	
Resolution range (Å)	20–2.1
Reflections	2868
R_{work} (%)	20.3 (22.8)
R_{free} (%)	23.3 (25.8)
Geometry	
Rmsd bonds (Å)	0.021
Rmsd angles (°)	2.8

[a] Values of the outermost bins are given in parentheses.

ning the length of the DNA crystals described here make this array an attractive choice for prototyping such applications. The channels created by the 13-mer are not large enough to accommodate proteins or large macromolecules, but they are large enough to accommodate small molecules or peptides. By contrast, modeling of the extended DNA lattice indicates that the solvent channels in these crystals could accommodate globular proteins as large as 45 kDa in a single unit cell (Figure 6D).

The 3′ end of each 13-mer is oriented into a channel and provides a convenient point for tethering guest molecules. We have successfully produced crystals with molecules containing from one to four additional 3′-terminal nucleotides, as well as molecules containing 3′-linked fluorophores and alkylthiol groups. These crystals diffract as well as unmodified crystals, but we have been unable to observe the guest molecules in difference density maps. This disorder is likely due to the guest molecules being present in many different orientations within the solvent channels. This finding highlights the importance of using well-defined environments for guest molecules in a scaffolded context; in the absence of such features, disorder results. One application not dependent on constant orientation may be as a molecular sieve for filtering molecules by size or capturing them with a 3′-linked affinity tag. The programmability of Watson-Crick base pairing has been a central principle in the construction of nanoscale DNA objects, but predictable non-Watson-Crick interactions can be a potentially powerful tool for the creation of diverse DNA nanostructures (e.g., [27]). For example, the motif described here could be used as a component in nanomechanical systems, similar to the non-Watson-Crick G4 motifs used previously [28, 29], or as a topological scaffold [30] with parallel features.

Significance

We have determined to excellent resolution the crystal structure of a continuously hydrogen bonded three-dimensional DNA lattice composed primarily of non-Watson-Crick base pairs. Due to their inherent programmability, the use of Watson-Crick base pairing has been a major tenet in the construction of nanoscale DNA objects; however, we show that non-Watson-Crick interactions also can be used predictably for the creation of well-structured DNA motifs. The observation of parallel-stranded homo base pairings in solution studies and in the crystal structure described here provides strong evidence for a predictable motif derived from these non-Watson-Crick pairs. One major goal of structural DNA nanotechnology has been the creation of designed three-dimensional DNA crystals. We have combined the non-Watson-Crick motif found here with Watson-Crick base pairing to create DNA crystals with predicted lattice dimensions. The DNA crystals described here could be used to prototype a variety of nanotechnological applications that include use as molecular sieves and as macromolecular scaffolds for structure determination of guest molecules or the assembly of molecular electronic materials. The motif by itself could be used as a component of nanomechanical devices or as a topological scaffold.

Experimental Procedures

Crystallization and Data Collection

The oligonucleotide, d(GGAC^{Br}AGAU^{Br}GGGAG), was synthesized using standard phosphoramidite chemistry. DNA molecules were purified by polyacrylamide gel electrophoresis and dialyzed against pure water. The DNA concentration was adjusted to 200 μM. Crystals were grown in batch mode by mixing 3 μl of DNA solution with 1 μl of 120 mM magnesium formate, 50 mM LiCl, and 10% MPD. Drops were incubated at 37°C overnight, after which the temperature was lowered to 27°C. Crystals shaped like hexagonal pyramids grew overnight to a size of 400 microns in the longest dimension. The lattice assembled in space group $P6_4$ with the dimensions a = b = 40.6 Å, c = 55.2 Å, containing a single 13-mer in the asymmetric unit. Data were collected at National Synchrotron Light Source beamline X8-C at 100 K. Anomalous data used in SAD phasing were collected at the maximum absorption edge of Br (0.9200 Å). Data were processed in HKL2000 [31].

Structure Determination and Refinement

Phasing was done by single-wavelength anomalous dispersion (SAD) using a 5-bromo deoxycytidine and 5-bromo deoxyuridine-modified oligonucleotide (Table 1). Refinement of heavy-atom positions using anomalous dispersion was carried out in CNS [32]. CNS was used to solvent-flatten electron density maps generated using the refined heavy-atom sites or the heavy-atom sites with the sign of the fractional coordinates flipped in space groups $P6_4$ and $P6_2$. The distinction of right- and left-handed helices was visible between the two space groups with clearly traceable phosphodiester backbones. The model was fit to the electron density using Xfit [33]. The base and ribose of G13 were not present in maps generated from experimental phases or maps using combined phases from partially or fully fit models. Refinement was initially carried out in CNS to an R factor = 25%, R_{free} = 28%, at which time the refinement was switched to REFMAC5 [34]. The same test set reflections were used with REFMAC5 to obtain the final R factors given in Table 1.

Molecular Modeling

Models of the two-part lattice were constructed manually in Xfit using B-form DNA output from 3DNA fused with the structural features described here. The model was built as a four-stranded dimer in space group $P3_1$ to avoid origin ambiguities and to maintain base pairing more easily when generating symmetry-related molecules. The unit cell was estimated to be a = b = 110.0 Å, c = 55.93 Å.

Acknowledgments

This research has been supported by grants from the National Institute of General Medical Sciences, the Office of Naval Research, the National Science Foundation, and DARPA/AFSOR to N.C.S. Additional support was provided to P.J.P. by an NIH grant to Alan Lambowitz. P.J.P. would like to thank Drs. Edward Marcotte and Andy Ellington for valuable discussions.

Received: May 3, 2004
Revised: May 19, 2004
Accepted: May 19, 2004
Published: August 20, 2004

References

1. Bong, D.T., and Ghadiri, M.R. (2001). Self-assembling cyclic peptide cylinders as nuclei for crystal engineering. Angew. Chem. Int. Ed. Engl. *40*, 2163–2166.
2. Shivanyuk, A., and Rebek, J., Jr. (2001). Reversible encapsulation by self-assembling resorcinarene subunits. Proc. Natl. Acad. Sci. USA *98*, 7662–7665.
3. Fenniri, H., Mathivanan, P., Vidale, K.L., Sherman, D.M., Hallenga, K., Wood, K.V., and Stowell, J.G. (2001). Helical rosette nanotubes: design, self-assembly, and characterization. J. Am. Chem. Soc. *123*, 3854–3855.
4. Seeman, N.C. (2003). DNA in a material world. Nature *421*, 427–433.
5. Mao, C., Sun, W., Shen, Z., and Seeman, N.C. (1999). A nanomechanical device based on the B-Z transition of DNA. Nature *397*, 144–146.
6. Yurke, B., Turberfield, A.J., Mills, A.P. Jr., Simmel, F.C. and Newmann, J.L. A DNA-fuelled molecular machine made of DNA (2000). Nature *406*, 62–65.
7. Yan, H., Zhang, X., Shen, Z., and Seeman, N.C. (2002). A robust DNA mechanical device controlled by hybridization topology. Nature *415*, 62–65.
8. Seeman, N.C. (1982). Nucleic acid junctions and lattices. J. Theor. Biol. *99*, 237–247.
9. Qiu, H., Dewan, J.C., and Seeman, N.C. (1997). A DNA decamer with a sticky end: the crystal structure of d-CGACGATCGT. J. Mol. Biol. *267*, 881–898.
10. Hagerman, P.J. (1988). Flexibility of DNA. Annu. Rev. Biophys. Biophys. Chem. *17*, 265–286.
11. Caruthers, M.H. (1985). Gene synthesis machines: DNA chemistry and its uses. Science *230*, 281–285.
12. Winfree, E., Liu, F., Wenzler, L.A., and Seeman, N.C. (1993). Design and self-assembly of two-dimensional DNA crystals. Nature *394*, 539–544.
13. Batey, R.T., Rambo, R.P., and Doudna, J.A. (1999). Tertiary motifs in RNA structure and folding. Angew. Chem. Int. Ed. Engl. *38*, 2326–2343.
14. Westhof, E., and Fritsch, V. (2000). RNA folding: beyond Watson-Crick pairs. Structure *8*, R55–R65.
15. Sundquist, W.I., and Klug, A. (1989). Telomeric DNA dimerizes by formation of guanine tetrads between hairpin loops. Nature *342*, 825–829.
16. Huertas, D., and Azorin, F. (1996). Structural polymorphism of homopurine DNA sequences. d(GGA)n and d(GGGA)n repeats form intramolecular hairpins stabilized by different base-pairing interactions. Biochemistry *35*, 13125–13135.
17. Peyret, N., Seneviratne, P.A., Allawi, H.T., and SantaLucia, J. (1999). Nearest-neighbor thermodynamics and NMR of DNA sequences with internal A.A, C.C, G.G, and T.T mismatches. Biochemistry *38*, 3468–3477.
18. Hermann, T., and Westhof, E. (1999). Non-Watson-Crick base pairs in RNA-protein recognition. Chem. Biol. *6*, R335–R343.
19. Privé, G.G., Yanagi, K., and Dickerson, R.E. (1991). Structure of the B-DNA decamer C-C-A-A-C-G-T-T-G-G and comparison with isomorphous decamers C-C-A-A-G-A-T-T-G-G and C-C-A-G-G-C-C-T-G-G. J. Mol. Biol. *217*, 177–199.
20. Lu, X.-J., and Olson, W.K. (2003). 3DNA: a software package for the analysis, rebuilding and visualization of three-dimensional nucleic acid structures. Nucleic Acids Res. *31*, 5108–5121.
21. Kettani, A., Bouaziz, S., Skripkin, E., Majumdar, A., Wang, W., Jones, R.A., and Patel, D.J. (1999). Interlocked mismatch-aligned arrowhead DNA motifs. Structure *7*, 803–815.
22. Robinson, H., van der Marel, G.A., van Boom, J.H., and Wang, A.H.-J. (1992). Unusual DNA conformation at low pH revealed by NMR: parallel-stranded DNA duplex with homo base pairs. Biochemistry *31*, 10510–10517.
23. Sunami, T., Kondo, J., Kobuna, T., Hiaro, I., Watanabe, K., Miura, K., and Takénaka, A. (2002). Crystal structure of d(GCGAAAGCT) containing a parallel-stranded duplex with homo base pairs and an anti-parallel duplex with Watson-Crick base pairs. Nucleic Acids Res. *30*, 5253–5260.
24. Chou, S.H., Zhu, L., and Reid, B.R. (1994). The unusual structure of the human centromere (GGA)2 motif. Unpaired guanosine residues stacked between sheared G.A pairs. J. Mol. Biol. *244*, 259–268.
25. Ribeiro, F.R., Alvarez, C., Henriques, C., Lemos, F., J.M. Lopes, and Ribeiro, M.F. (1995). Structure-activity relationship in zeolites. J. Mol. Catal. A Chem. *96*, 245–270.
26. Robinson, B.H., and Seeman, N.C. (1987). The design of a biochip: a self-assembling molecular-scale memory device. Protein Eng. *1*, 295–300.
27. Jaeger, L., Westhof, E., and Leontis, N.B. (2001). Tecto-RNA: modular assembly units for the construction of RNA nanoobjects. Nucleic Acids Res. *29*, 455–463.
28. Li, J.J., and Tan, W. (2002). A single DNA molecule nanomotor. Nano Lett. *2*, 315–318.
29. Alberti, P., and Mergny, J.-L. (2003). A DNA duplex-quadruplex exchange as the basis for a nanomolecular machine (2003). Proc. Natl. Acad. Sci. USA *100*, 1569–1573.
30. Zhu, L., Lukeman, P.S., Canary, J.W., and Seeman, N.C. (2003). Nylon/DNA: single-stranded DNA with a covalently stitched nylon lining. J. Am. Chem. Soc. *125*, 10178–10179.
31. Otwinowski, Z., and Minor, M. (1997). Processing of X-ray diffraction data collected in oscillation mode. Methods Enzymol. *276*, 307–326.
32. Brünger, A.T., Adams, P.D., Clore, G.M., DeLano, W.L., Gros, P., Grosse-Kunstleve, R.W., Jiang, J.S., Kuszewski, J., Nilges, M., Pannu, N.S., et al. (1998). Crystallography and NMR system: a new software suite for macromolecular structure determination. Acta Crystallogr. D Biol. Crystallogr. *54*, 905–921.
33. McRee, D.E. (1992). XtalView: a visual protein crystallographic software system for XII/Xview. J. Mol. Graph. *10*, 44–47.
34. Murshudov, G.N., Vagin, A.A., and Dodson, E.J. (1997). Refinement of macromolecular structures by the maximum-likelihood method. Acta Crystallogr. D Biol. Crystallogr. *53*, 240–255.
35. Merritt, E.A., and Bacon, D.J. (1997). Raster3D: photorealistic molecular graphics. Methods Enzymol. *277*, 505–524.

Accession Numbers

The atomic model and structure factors have been deposited in the Protein Data Bank (accession number 1P1Y).